RESEARCH

Hydrological and biogeochemical controls on temporal variations of dissolved carbon and solutes in a karst river, South China

Jing Liu[1], Jun Zhong[2]* , Shuai Chen[3], Sen Xu[2] and Si-Liang Li[2]

Abstract

Background: Understanding the responses of riverine dissolved carbon dynamics and chemical weathering processes to short-term climatic variabilities is important to understand the Surface-Earth processes under ongoing climate change. Temporal variations of solutes and stable carbon isotope of dissolved inorganic carbon ($\delta^{13}C_{DIC}$) were analysed during a hydrological year in the Guijiang River, South China. We aimed to unravel the chemical weathering processes and carbon dynamics in karst areas under ongoing climate changes.

Results: Significant positive relationships were found between weathering rates and climatic factors (i.e. temperature and discharge) over the hydrological year. The total flux of CO_2 consumption (760.4×10^3 mol/km²/year) in the Guijiang River was much higher than the global mean flux, with a higher CO_2 consumption capacity in the Guijiang River relative to most other global rivers. Chemical weathering fluxes in this karst area showed high sensitivity to global climate change. CO_2 evasion during the warm–wet seasons was much lower than those during cold–dry seasons. Light $\delta^{13}C_{DIC}$ values occurred under high-flow conditions, corresponding with the high temperatures in high-flow seasons. IsoSource modelling revealed that biological carbon could account for 53% of all dissolved inorganic carbon (DIC), controlling the temporal carbon variabilities.

Conclusion: This study quantitatively evaluated the temporal variations in CO_2 fluxes and carbon cycling of karstic river systems and demonstrated that riverine carbon cycling will have a higher sensibility to ongoing global climate change. High discharges accelerate solutes transport, with relatively large quantities of ^{13}C-depleted carbon being flushed into rivers. Meanwhile, high temperatures also accelerate organic carbon mineralisation, producing high content of soil CO_2, whose influx can shift the ^{13}C-depleted values in the high-flow seasons. Taken together, biological carbon influx should be responsible for the temporal carbon dynamics.

Keywords: Dissolved carbon, Karst landscape, $\delta^{13}C_{DIC}$, CO_2 outgassing, Carbon cycling

Background

Understanding the responses of carbon cycling to short-term climate variabilities (i.e. temperature and discharge) is necessary to investigate the effects of future global climate change on Surface-Earth processes [1, 2]. Of the different components within the global carbon cycle, the river system is the key channel, transporting dissolved carbon from the continents to the oceans [3]. Rock weathering is one of the main sources of dissolved carbon in river systems, which could consume atmospheric CO_2 by converting it into dissolved inorganic carbon (DIC). Therefore, chemical weathering processes have a significant effect on modulating atmospheric CO_2, and thereby affect global climate change.
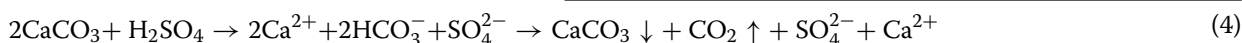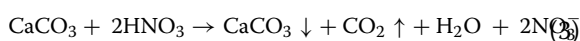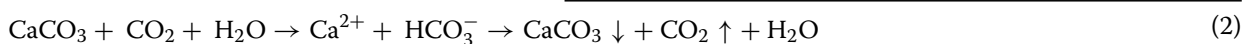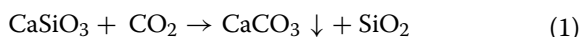
Silicate weathering involves carbonic acid and leads to the net sequestration of CO_2, which can be defined by Eq. (1). Carbonate rocks cover approximately 12%

*Correspondence: jun.zhong@tju.edu.cn
[2] Institute of Surface-Earth System Science, School of Earth System Science, Tianjin University, Tianjin 300072, China
Full list of author information is available at the end of the article

Liu *et al. Environ Sci Eur*   (2021) 33:53

Page 2 of 15

of the Earth's ice-free land area [4], with thin soil cover and well-developed conduit networks forming large underground drainage systems [5]. The dissolution of carbonate rocks consumes ~0.15 Pg of atmospheric CO_2 each year, based on the geochemical data from large rivers worldwide [6]. And the produced DIC is then transported to the ocean, which plays an important role as a carbon sink. On the other hand, as carbonate weathering can be consumed by other acids (e.g. nitric, sulfuric, and organic acids), it can lead to CO_2 release rather than CO_2 consumption [7], which can be expressed as Eqs. (3 and 4).

$$CaSiO_3 + CO_2 \rightarrow CaCO_3 \downarrow + SiO_2 \tag{1}$$

$$CaCO_3 + CO_2 + H_2O \rightarrow Ca^{2+} + HCO_3^- \rightarrow CaCO_3 \downarrow + CO_2 \uparrow + H_2O \tag{2}$$

$$CaCO_3 + 2HNO_3 \rightarrow CaCO_3 \downarrow + CO_2 \uparrow + H_2O + 2NO_3^- \tag{3}$$

$$2CaCO_3 + H_2SO_4 \rightarrow 2Ca^{2+} + 2HCO_3^- + SO_4^{2-} \rightarrow CaCO_3 \downarrow + CO_2 \uparrow + SO_4^{2-} + Ca^{2+} \tag{4}$$

In addition to delivering a large amount of DIC to the oceans, rivers also release CO_2 into the air through the water–air interface [8]. Raymond et al. [9] reported that global CO_2 emissions from inland waters to the atmosphere is approximately equal to 2.1 Pg of C per year. Hence, it is important to conduct extensive research on both the vertical and lateral transport of DIC in river systems, especially the transference of carbon in the lithosphere, hydrosphere, and atmosphere [10–13].

The riverine DIC is generally affected as follows: (1) the weathering of carbonate/silicate rocks, (2) soil CO_2 produced by the organic matter decomposition, and (3) the exchange of CO_2 at the water–air interface [2, 14]. Each source/process is involved in the carbon cycle, which could be traced using $\delta^{13}C_{DIC}$ combined with the dissolved carbon contents [15, 16]. For marine carbonate bedrock sources, $\delta^{13}C$ values are typically 0‰ (Vienna Pee Dee Belemnite) [17]. The $\delta^{13}C$ values of plants are controlled by specific photosynthetic paths, involving the pathways of the Calvin cycle (C_3) and the Hatch–Slack (C_4). These C_3 and C_4 plants induce different carbon isotopic fractionation, with $\delta^{13}C$ of the CO_2 are $-27‰$ and $-13‰$ (VPDB), respectively [17]. Due to the relative difference in the partial pressure of CO_2 (pCO_2) of the river and overlying atmosphere, CO_2 evasion causes ^{13}C-enriched in the residual DIC. Related studies have reported that rivers are usually supersaturated to atmospheric CO_2, leading to vertical CO_2 degassing to the atmosphere [18, 19]. For example, African inland rivers degassed 0.27–0.37 Pg C/year into the atmosphere [20].

Chemical weathering and related CO_2 consumption fluxes are highly affected by hydrological conditions. However, the coupled effects of hydrological and biogeochemical processes on CO_2 fluxes in river systems remain unclear. For example, the fluxes of CO_2 consumption are calculated by discharge and the dissolved solute content, yet the covariation between the above two variables could induce great uncertainty [21]. Additionally, seasonal and diurnal variations in CO_2 degassing may result from differences in solar radiation and temperature, causing changes in the content of DIC and CO_2 [22]. Thus, to reduce the overall uncertainty, high-frequency (monthly or even daily scales) sampling and analyses of hydrochemistry, isotopes, synchronous hydrology and meteorology of river systems are required.
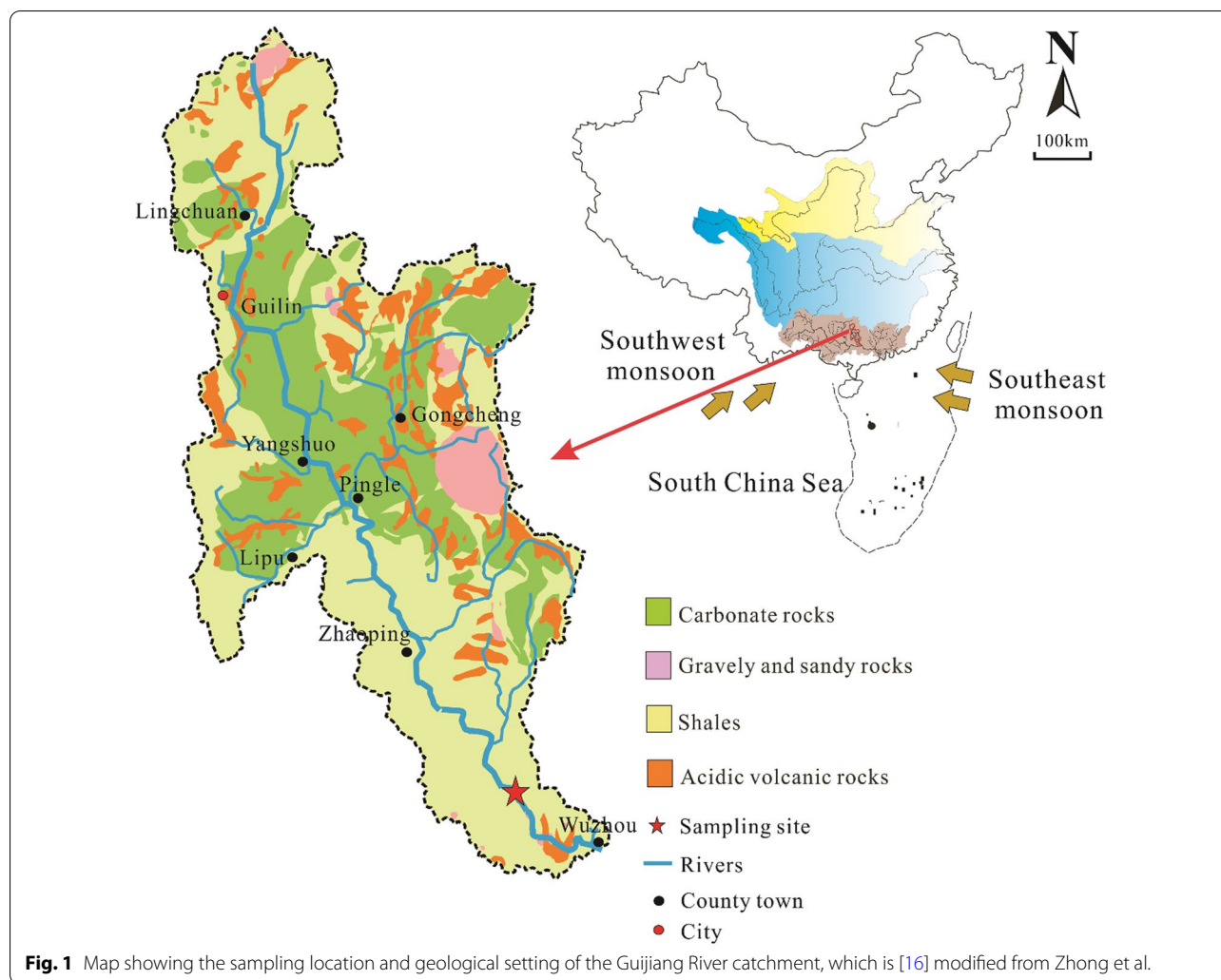
The Guijiang River catchment is located in Southwest China, which is one of the largest karst regional centers in the world, exhibiting a high sensibility responding to chemical weathering processes under changing climate conditions. It is an ideal study object to understand carbon dynamics and weathering processes in response to various climatic conditions in karst rivers. Here, the Guijiang River catchment was selected to analyse the high-frequency contents of dissolved solutes and $\delta^{13}C_{DIC}$, aiming to (1) depict the temporal variations of solute dynamics in a typical karstic catchment; (2) obtain information on the fluxes of chemical weathering and CO_2 consumption in response to climatic variabilities; (3) quantify the potential sources of DIC; and (4) estimate the vertical CO_2 fluxes from surface waters into the atmosphere.

Materials and methods
Site description and data source
The Guijiang River catchment (23° 28′–23° 55′ N, 110° 05′–110° 29′ E) is located in the northeastern Guangxi Province of South China. The study catchment has a length of 426 km from north to south, with a drainage area of 19,288 km^2. It originates from the Maoer Mountain, with an elevation of approximately 2141 m, and then flows southward through Guilin, where a typical karstic landscape is developed, finally entering the Xijiang River. Its landscape contains mainly hills and mountains with significant topographic relief. Karstic topography in the study catchment is well-developed (Fig. 1). Specifically, the upper–middle catchment is dominated by Permian

Fig. 1 Map showing the sampling location and geological setting of the Guijiang River catchment, which is [16] modified from Zhong et al.

and Triassic carbonate rocks including sulfide-rich limestones and dolomites. The bedrocks distributed in the middle–lower catchment area are mainly Precambrian metamorphic rocks (gneiss) and igneous rocks (primarily granite). Few evaporites are scattered throughout the Guijiang River catchment, and no salt-bearing strata have been discovered [23–25].

The whole catchment is controlled by the subtropical monsoon climate. Here, the total annual precipitation varies from 1900 to 2700 mm, and most of the rainfall events (~80%) occur in the rainy season (April–September), while the mean annual temperature is ~19–21 °C [26, 27]. The study catchment is mainly hilly (40.8%) and highland (42.8%), has a low to medium degree of erosion, with a mean soil erosion rate of 157.7 t km^{-2} year^{-1} [28]. The main types of land use are forests (67.3%) and cultivated lands (10.8%) [28].

The sampling site was situated at the outlet of the Guijiang River (Fig. 1), which is ~39 km away from the mainstream of the Xijiang River. We collected 8 river water samples from October of 2013 to May of 2014 on monthly intervals during the low-flow season, while from June to September of 2014, 23 river water samples were collected based on the changing discharge conditions during the high-flow season. The sampling and analysis method for the content of major ions, dissolved organic carbon (DOC), and carbon isotopes ($\delta^{13}C_{DIC}$) were same to Liu et al.'s study [29]. Daily river discharge (Q) was collected online from the Ministry of Water Resources (http://www.hydroinfo.gov.cn/), while water surface evaporation (WSE), water temperature (WT), daily precipitation (DP), and suspended sediment loads (SSL) were collected from the Hydrological Yearbook published by the Pearl River Conservancy Commission [30, 31].

Liu *et al. Environ Sci Eur*   (2021) 33:53

Page 4 of 15

Data analysis
LOADEST modelling
The fluxes of major ions, DIC, and DOC contents with corresponding daily Q were estimated by the Load Estimator (LOADEST) [32], which was performed using LoadRunner software [33]. According to the Akaike information criterion (AIC) in LOADEST [33], the following model was selected to calculate the daily loads of dissolved solutes and DIC:

$$\text{In Load} = a_0 + a_1 \text{In}Q + a_2\sin(2\pi\,\text{dtime}) + a_3\cos(2\pi\,\text{dtime}) + a_4\text{dtime}, \tag{5}$$

while the DOC loads estimation uses the following model:

$$\text{In Load} = a_0 + a_1\text{In}Q + a_2\ln\left(Q^2\right) + a_3\sin(2\pi\,\text{dtime}) + a_4\cos(2\pi\,\text{dtime}) + a_5\text{dtime} + a_6(\text{dtime})^2, \tag{6}$$

where *Load* is the content of constituents (kg/days), a_0 to a_6 are the model coefficients, dtime and Q indicate the centre of decimal time and discharge, respectively. The LOADEST conducts calibrations and calculates fluxes based on an Approximate Maximum Likelihood Estimation (AMLE) algorithm. The values of $\delta^{13}C_{DIC}$ were calculated based on the estimated HCO_3^- content.

The concentration–discharge (C–Q) relationships
The C–Q relationships of riverine materials express the transport and reactions of dissolved loads with changing discharge in catchments [13, 34, 35]. In this study, a power-law function was fitted to express the C–Q relationships as follows:

$$C = a \times Q^b, \tag{7}$$

where b is an index for mirroring the behaviors of solutes in response to discharge variabilities. If $b \approx 0$, C is equal to the constant a, independent of variations in Q; when $-1 < b < 0$, dilution and chemostatic behaviors coexist. When $b = -1$, the solute content decreases with high water flux, and Q is the only control on C, while if $b > 0$, the solute content increases as water flux increases and shows a flushing behavior.

The coefficients of variation of the solute contents and Q (CV_C/CV_Q) are helpful to delineate the behaviors of solute contents responding to various water fluxes [36], and can be expressed as follows:

$$CV_C/CV_Q = (\mu_Q\sigma_C) / (\mu_C\sigma_Q), \tag{8}$$

where μ_C and μ_Q are the average values of solute contents and discharges, σ_C and σ_Q are their standard deviations.

Chemostatic behavior ($b \approx 0$, $CV_C/CV_Q << 1$) can be defined as the buffering of variations in content as compared to the null hypothesis.

Calculation of the calcite saturation, pCO2 and FCO2
The calcite saturation index (SIc) and pCO_2 of water samples were calculated by mass action relationships described by water temperatures and corresponding thermodynamic constants [17]. The evasion of CO_2 from surface water to the atmosphere will happen when pCO_2 values of the river water are much larger than those in the ambient air. For the studied river, the CO_2 diffusion flux can be calculated as follows:

$$F_{CO_2} = k \times K_H \times \left(pCO_{2(aq)} - pCO_{2(air)}\right), \tag{9}$$

where F_{CO_2} (mmol/m^2/days) denotes the diffusion flux of CO_2 across the water–air interface, k is the gas exchange rate (cm/h), K_H represents Henry's constant, $pCO_{2(aq)}$ and $pCO_{2(air)}$ are the partial pressure of CO_2 at the water surface and atmosphere. If $F_{CO_2} > 0$, CO_2 fluxes evasion from the water to the atmosphere, while if $F_{CO_2} < 0$, CO_2 invasion from atmosphere to water. 400 µatm for atmospheric CO_2 content was employed, and k represents a temperature-dependent Schmidt number (Sc_T) of fresh water,

$$k = k_{600} \times (600/Sc_T)^{0.5} \tag{10}$$

With

$$Sc_T = 1911.1 - 118.11T + 3.4527T^2 - 0.04132T^3 \tag{11}$$

where T represents the in situ water temperature (°C), and k_{600} represents the k for CO_2 at 20 °C in fresh water. The value of k depends on river size [37], which is generally divided into two kinds, one is for the small river with a channel < 100 m, while the other is for the large river with a channel > 100 m. The main channel of the Guijiang River width is usually > 100 m, so $k_{600} = 4.46 + 7.11 \times u_{10}$ (u_{10} represents the average wind speed at 10 m above rivers) was employed here. During the sampling period, the wind speed at Wuzhou ranged from 1.2 to 2.9 m/s, averaging 1.8 m/s, showing constant with previous related research [18, 19, 37].

Results

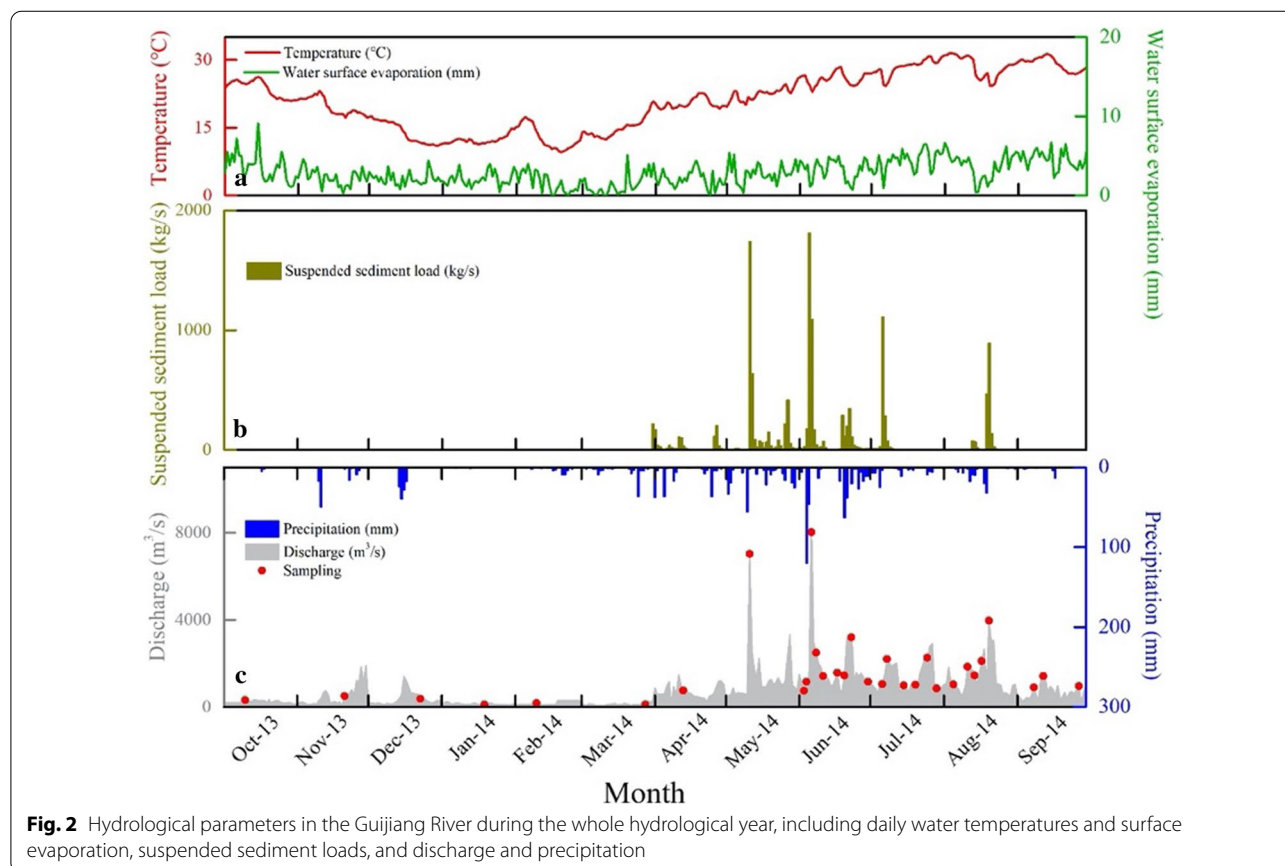### Hydrological parameters and hydrochemical characteristics

The hydrological parameters for the Guijiang River catchment are shown in Fig. 2. At the Pingle hydrological station, the WT records showed significant seasonal variations that followed meteorological trends. The highest WT reached 31.5 °C in the wet season, and intense evaporation at the water surface was in accordance with the high-temperature conditions (Fig. 2). In the dry season, as the WT dropped, evaporation at the water surface decreased accordingly. River water discharge was low in October of 2013, reaching two small peaks in November and December, and then declining rapidly and stabilizing at a minimal discharge from January to March of 2014. In April of 2014, there was a third small peak. Subsequently, discharge fluctuated mainly in the wet period, and reached its largest peak in June of 2014. The SSL also presented similar patterns with variations in discharge.
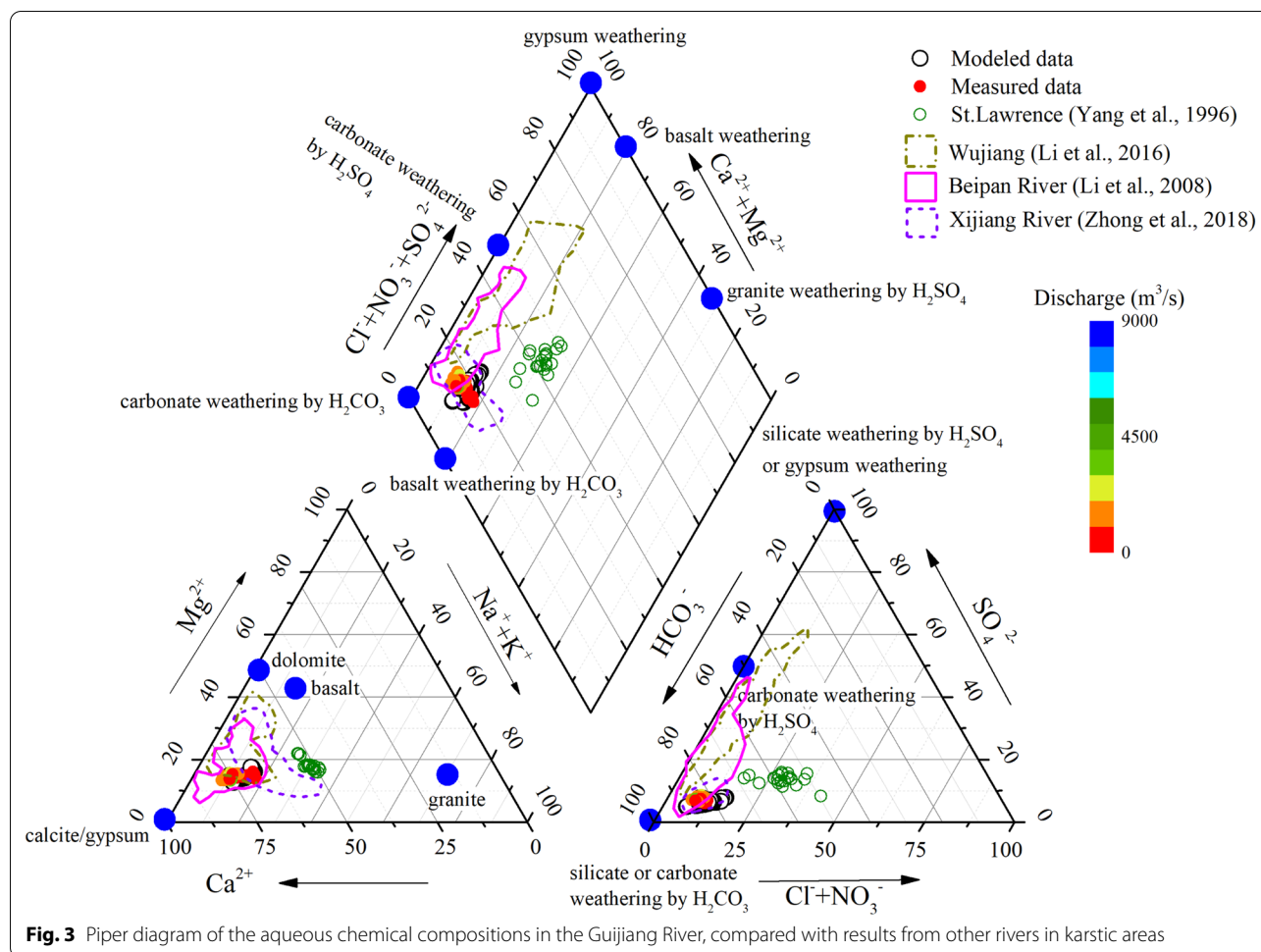
EC values had a wide range changing from 121 to 210 μS/cm, with a mean of 150 μS/cm. The amount of total dissolved solids (TDS) varied from 105 to 185 mg/L, with a mean discharge-weighted content (MDWC=$\sum(C \times Q)/\sum Q$, where C represents the

riverine solute content, and Q indicates the instantaneous discharge) of 118 mg/L, higher than the global discharge-weighted mean (97 mg/L) [38]. TZ^+ is the total cationic charge ($TZ^+=2Ca^{2+}+2Mg^{2+}+Na^++K^+$), and TZ^- is the total anionic charge ($TZ^-=HCO_3^-+2SO_4^{2-}+NO_3^-+Cl^-$). The normalized ionic charge balances (NICB=[(TZ^+-TZ^-) × 100%]/(TZ^++TZ^-)) were well-balanced (below 5%), implying that the unanalyzed ions amounted to negligible proportions. The MDWC values of cations were as follows, Ca^{2+} (22.7 mg/L) > Mg^{2+} (2.6 mg/L) > Na^+ (1.3 mg/L) > K^+ (0.9 mg/L), with the sum of Ca^{2+} and Mg^{2+} accounting for 94% of TZ^+. Meanwhile, the MDWC values of anions were as follows, HCO_3^- (67.9 mg/L) > SO_4^{2-} (9.3 mg/L) > NO_3^- (3.9 mg/L) > Cl^- (2.0 mg/L), with the sum of HCO_3^- and SO_4^{2-} accounting for 91% of TZ^-. The Guijiang River yielded a predominance of HCO_3^-, SO_4^{2-}, Ca^{2+}, and Mg^{2+}, consistent with other karstic rivers (Fig. 3) [13, 14, 16, 27, 39].

Characteristics of dissolved carbon

In this study, the DOC contents fluctuated between 0.7 mg/L in the wet season and 2.4 mg/L in the dry season, with the *MDWC* value of 1.3 mg/L. Most of
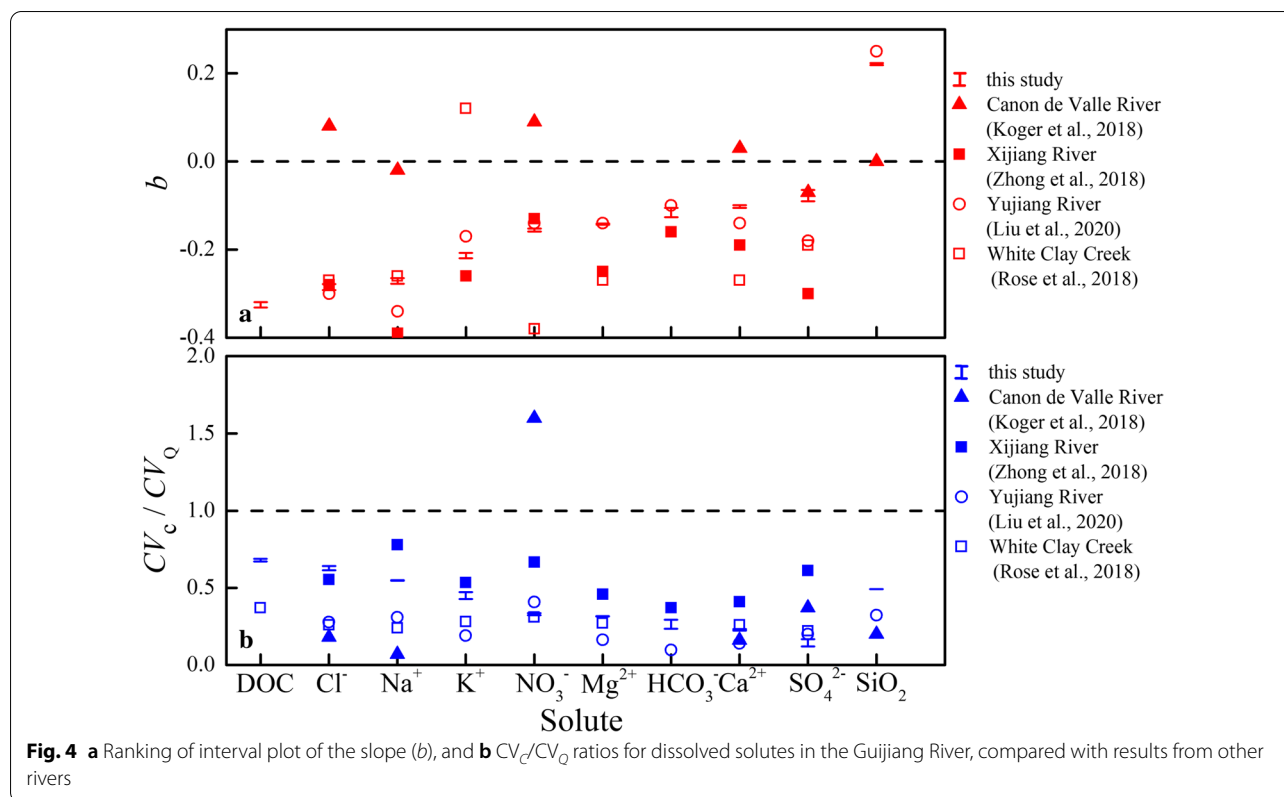

Fig. 2 Hydrological parameters in the Guijiang River during the whole hydrological year, including daily water temperatures and surface evaporation, suspended sediment loads, and discharge and precipitation

Fig. 3 Piper diagram of the aqueous chemical compositions in the Guijiang River, compared with results from other rivers in karstic areas

the river water samples contained less than 2 mg/L of DOC. Among the DIC species (i.e. carbonate (CO_3^{2-}), HCO_3^-, carbonic acid (H_2CO_3), and $CO_{2(aq)}$), HCO_3^- was the predominant component, accounting for 95% (range of 84–98%) of DIC. The values of $\delta^{13}C_{DIC}$ ranged from $-16.9‰$ during the wet season to $-9.2‰$ during the dry season (mean $-13.6‰$), exhibiting distinct temporal variations. The pCO_2 values ranged from 727 µatm to 6580 µatm, with a mean value of 1866 µatm, which were generally greater than the atmospheric pCO_2. The calcite saturation index (SIc) ranged from approximately $10^{-3.4}$ to $10^{-2.9}$ (mean $10^{-3.2}$). All river water samples had SIc values of >0, and water samples were oversaturated with respect to calcite. F_{CO2} values showed seasonal variations and ranged from 23 mmol/m²/days (May of 2014) to 264 mmol/m²/days (Jan of 2014), averaging 84 mmol/m²/days in the study river.

Discussion

Solute behaviors to hydrological variabilities

For the Guijiang River, the content of most solutes displayed negative power-law relationships with discharge (Fig. 4a), showing that most solutes decreased with increasing discharge. However, $CV_C/CV_Q < 1$ indicates that although the C–Q relationships showed different behaviors, the total solute content exhibited much less variability in response to changes in discharge (Fig. 4b). Geogenic ions (e.g. Ca^{2+}, Mg^{2+}, HCO_3^-, Na^+, and K^+) consistently showed dilution but chemostatic behaviors in the study river, which are similar to those in the Xijiang River and Yujiang River [16, 29]. Ions from carbonate rocks (e.g. Ca^{2+}, Mg^{2+}, and HCO_3^-) showed intense chemostatic behaviors when compared to those from silicate weathering (e.g. Na^+ and K^+), which may be due to the rapid kinetics of carbonate rock weathering [40]. Meanwhile, Na^+ and K^+ exhibited significant dilution patterns,

Fig. 4 **a** Ranking of interval plot of the slope (*b*), and **b** CV_C/CV_Q ratios for dissolved solutes in the Guijiang River, compared with results from other rivers

with higher CV_C/CV_Q ratios and more negative *b* values compared to Ca^{2+}, Mg^{2+}, and HCO_3^-, suggesting that ions from silicate weathering have a higher sensibility to increasing water flux when compared to carbonate-sourced ions [16]. Another important source of K^+ was associated with the cation exchange between water and soil [40], especially during storm events [35]. Cl^- yielded lower *b* values and higher CV_C/CV_Q ratios, suggesting that Cl^- showed the strongest dilution effects among all solutes. The C–Q relationship for SiO_2 exhibited a slight flushing behavior, indicating that variations in discharge had little impact on variations in SiO_2 content, which is associated with secondary mineral precipitation [16]. A weathered zone can store or accumulate silica, until rapid flushing of the weathered zone by storm pulses induces dissolution and entrainment in rivers [41–43]. The C–Q patterns of SO_4^{2-} and NO_3^- showed similar behaviors, and both of them were greatly affected by anthropogenic inputs and biological activities. Sulfide-rich minerals in coal-bearing deposits within the bedrock formations underlay the study area, which serves as a geological source of SO_4^{2-} in this catchment [39]. Exogenous sources are often linked with SO_4^{2-} and NO_3^-, which are generally correlated with chronic and elevated atmospheric precipitation, or with the application of chemical fertilizers during agricultural activities [35]. The Guijiang

River catchment lies in South China, which is subject to intense acid rain [39, 44]. Additionally, it has been reported that the nitrogen fertilizer consumption budget accounted for $\sim (7.25–7.47) \times 10^8$ kg·N·year^{-1} from 2012 and 2014 [45]. Biologically associated solutes, such as DOC, further yielded the lowest CV_C/CV_Q and most negative *b*, presented in Fig. 4b, showing a similar dilution behavior, and implying that the variability in DOC content was also predominantly controlled by variations in discharge in this study area.
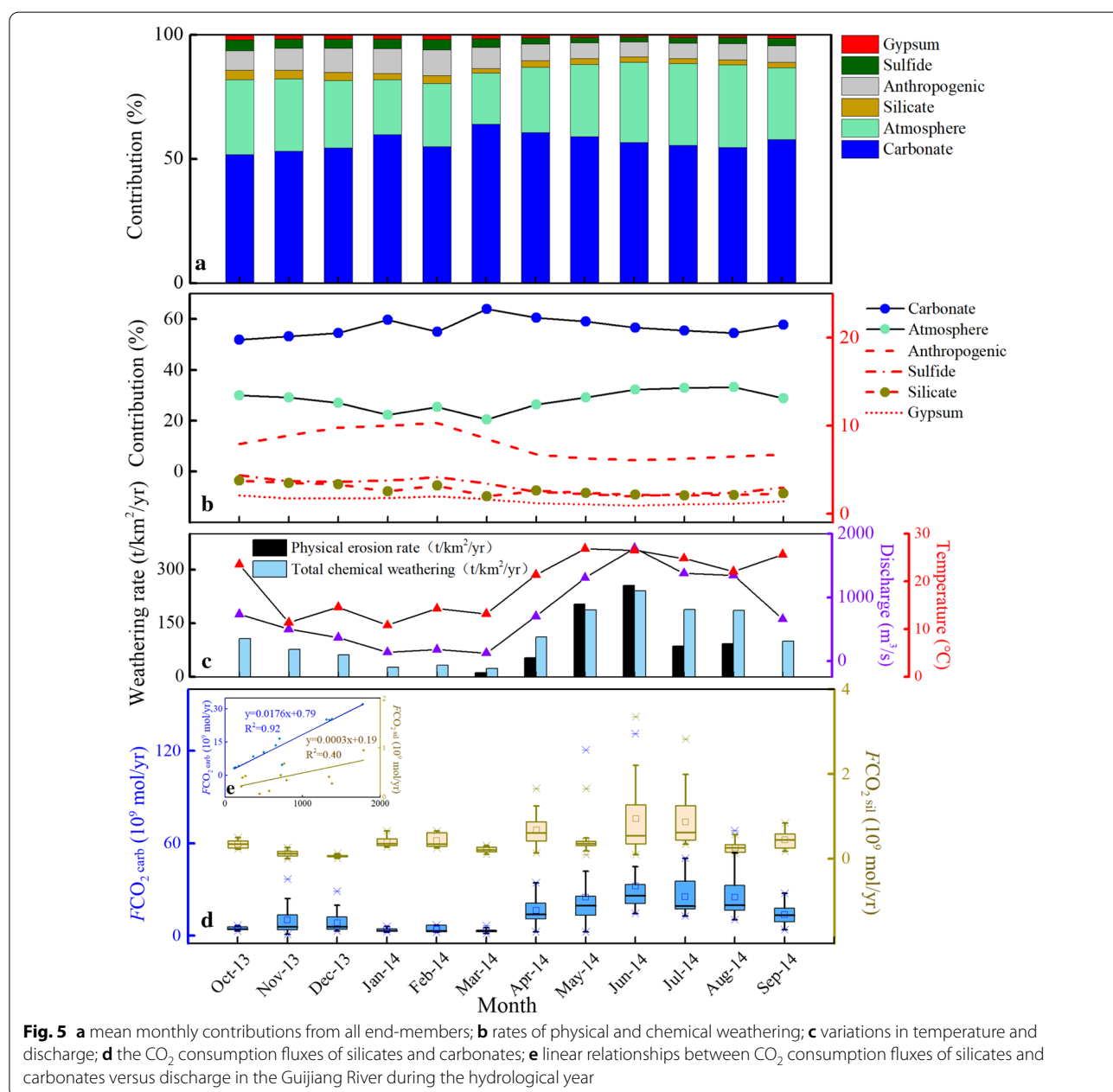
Responses of weathering processes to climatic variabilities

Riverine materials are mainly sourced from atmosphere inputs, rocks weathering, and anthropogenic activities (e.g. coal combustion). Based on the forward model using Additional file 1: Eqs. (S1–S10), we found that dissolved solutes in this studied river were mainly derived from carbonate weathering, which accounted for a mean of 56.8% of total cations in the Guijiang River, followed by atmospheric inputs (28.1%), anthropogenic activities (7.8%), sulfide oxidation (3.1%), silicate weathering (2.6%), and gypsum dissolution (1.5%). The contributions of sulfide oxidation and gypsum dissolution were generally <5% in this study area.

For most end-members, especially atmospheric inputs and silicate weathering, the contributions

Liu *et al. Environ Sci Eur* (2021) 33:53

Page 8 of 15

generally showed significant dilution behavior in response to increases in discharge. Meanwhile, the percentage of carbonate sources was shown to be relatively stable for the hydrological year (Figs. 5a, b). These behaviors can be attributed to the dissolution kinetic characters of carbonate weathering, which may be enhanced by the generation of soil CO_2 and associated biological processes under warm and wet conditions [46]. Similar observations have been reported in monsoonal rivers worldwide [16, 47].

The products of silicate weathering, such as, Ca^{2+}, Mg^{2+}, Na^+, K^+, and dissolved SiO_2, were used to calculate the silicate weathering rate (SWR), while the Ca^{2+}, Mg^{2+}, and HCO_3^- contents from carbonate dissolution produced by carbonic and sulfuric acids were used to estimate the carbonate weathering rate (CWR). The equations for these rates are presented in Additional file 1 as equations (S11) and (S12), respectively. The SWR ranged from 0.4 t/km^2/year in the dry period to 78.6 t/km^2/year in the wet period, averaging 6.5 t/km^2/year, which was lower than the River Rhône (14.4 t/km^2/year)

Fig. 5 **a** mean monthly contributions from all end-members; **b** rates of physical and chemical weathering; **c** variations in temperature and discharge; **d** the CO_2 consumption fluxes of silicates and carbonates; **e** linear relationships between CO_2 consumption fluxes of silicates and carbonates versus discharge in the Guijiang River during the hydrological year

[47] and Yujiang (7.6 t/km^2/year) [29], but much higher than the River Seine (1.2–2.6 t/km^2/year) [48]. Simultaneously, the CWR ranged from 5.8 t/km^2/year in the dry period to 802.5 t/km^2/year in the wet period, averaging 88.1 t/km^2/year, which was also higher than the River Seine (48 t/km^2/year) [48] and Yujiang (69.7 t/km^2/year) [29], but was similar to the River Rhône (89 t/km^2/year) [47]. The results suggest that to reduce the uncertainties in *SWR* and *CWR* estimations, high-frequency temporal sampling strategies and geochemical analyses with synchronous discharge are necessary.

The average total chemical weathering rate (TWR = CWR + SWR) in this study was 105.9 t/km^2/year, much higher than the global mean (24 t/km^2/year) [15], but lower than the value reported in a previous study (129 t/km^2/year) [27]. The mean rate of physical erosion was 148.0 t/km^2/year, which increased by ten or even hundreds of times relative to the TWR in the wet period. However, there were significant positive relationships between the total weathering rates (i.e. rates of physical erosion and chemical weathering) and variabilities of temperatures and discharge over the hydrological year (Fig. 5c), consistent with the observations in the Yujiang River [29]. The reason for this is that high discharge accelerates the transport of suspended sediments and further exposes reactive mineral surfaces. Meanwhile, high temperatures accelerate biological activities, which may enhance soil CO_2 content, thereby accelerating rock weathering in the catchment [16]. Hence, physical and chemical weathering are two complementary processes at the catchment-scale controlling the morphology of the Earth's surface [16, 49]. Coupled physical and chemical weathering processes in crushed rocks provide weathered rocks and chemically reactive surfaces are easily fractured under various climatic conditions [49]. Additionally, biogeochemical processes are modified by physical processes, so dissolved solutes present diverse behaviors in response to variations in climatic conditions (i.e. discharge and temperature) [13, 50].

The CO_2 consumption fluxes from carbonate weathering (FCO$_{2carb}$) and silicate weathering (FCO$_{2sil}$) were deducted from the sulfuric acid involved with carbonate and silicate weathering, described by Additional file 1: Equations (S13 and S14), respectively. The mean monthly FCO$_{2carb}$ values showed strong positive relationships with discharge and temperatures, increasing from 3.2 × 10^9 mol/year (March of 2014) to 32.2 × 10^9 mol/year (June of 2014), averaging 14.3 × 10^9 mol/year, as shown in Figs. 5d, e. Meanwhile, FCO$_{2sil}$ values increased from 0.1 × 10^9 mol/year (December of 2013) to 0.9 × 10^9 mol/year (June of 2014), averaging 0.4 × 10^9 mol/year, which displayed positive relationships with changing discharge and temperatures during the hydrological

year (Figs. 5d, e). These findings showed that the FCO$_{2carb}$ had a higher sensitivity to variations in temperature and discharge relative to FCO$_{2sil}$, exhibiting similar behaviors with the contributions of silicate and carbonate weathering in response to changing discharge and temperature conditions. The FCO$_{2carb}$ and FCO$_{2sil}$ for the Guijiang River accounted for around 0.1% and 0.01% of the global CO_2 consumption fluxes by carbonate and silicate rocks weathering, respectively [6]. These results in this study were much lower than those previously reported (e.g. 21.1 × 10^9 mol/year and 1.86 × 10^9 mol/year) [27], which may be due to the uncertainties caused by limited sampling frequency in the previous study.
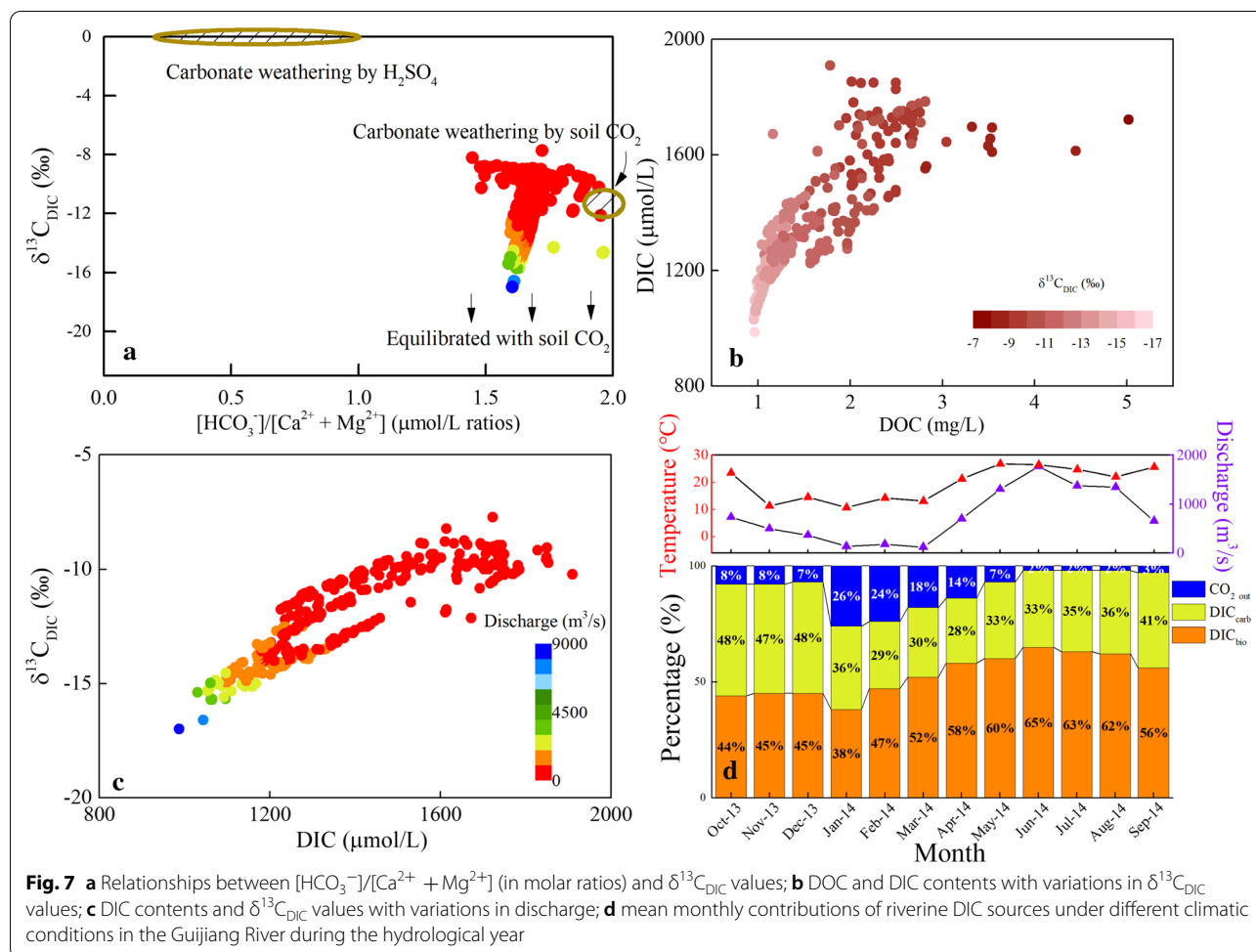
The total rates of CO_2 consumption (ΦCO_2 = $[\Phi CO_2]_{sil}$ + $[\Phi CO_2]_{carb}$) were defined as FCO$_2$ per unit area. Although the total ΦCO_2 (760.4 × 10^3 mol/km^2/year) do not show obvious advantages in those of global catchments, the CO_2 consumption capacity in this study river was much higher than the global mean (Fig. 6). Worldwide, rivers with large catchment areas generally had lower ΦCO_2, while rivers yielding higher ΦCO_2 values usually had small areas and low discharges [6]. The Changjiang River, Huanghe River, and the Xijiang River were all located near the global mean line [6].

Carbon dynamics under various climate variabilities

Previous studies had demonstrated that carbonate weathering via carbonic and sulfuric acids generated a large amount of DIC in karst areas [27]. Carbonate weathering involving carbonic and sulfuric acids may also lead to different elemental ratios, with the molar ratios of $[HCO_3^-]/[Ca^{2+} + Mg^{2+}] = 2$ or 1 [46]. As shown in Fig. 7a, carbonate weathering involved with carbonic acid
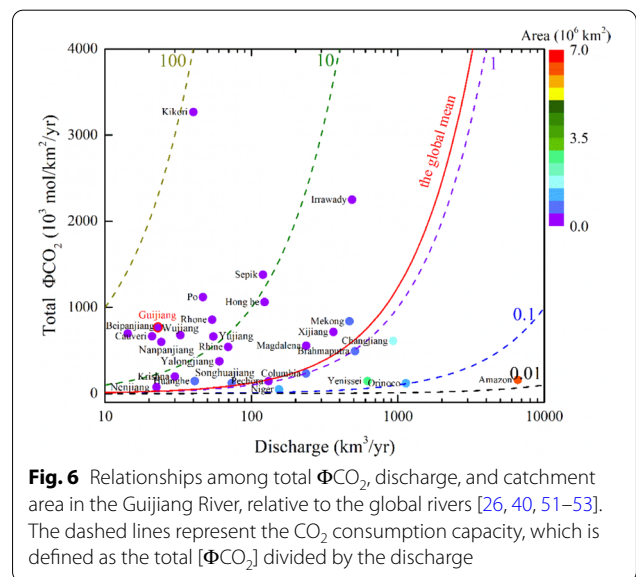
Fig. 6 Relationships among total ΦCO_2, discharge, and catchment area in the Guijiang River, relative to the global rivers [26, 40, 51–53]. The dashed lines represent the CO_2 consumption capacity, which is defined as the total $[\Phi CO_2]$ divided by the discharge

Liu *et al. Environ Sci Eur* (2021) 33:53

Page 10 of 15

Fig. 7 a Relationships between $[HCO_3^-]/[Ca^{2+} + Mg^{2+}]$ (in molar ratios) and $\delta^{13}C_{DIC}$ values; **b** DOC and DIC contents with variations in $\delta^{13}C_{DIC}$ values; **c** DIC contents and $\delta^{13}C_{DIC}$ values with variations in discharge; **d** mean monthly contributions of riverine DIC sources under different climatic conditions in the Guijiang River during the hydrological year

was the primary reaction, though sulfuric acid also acted an important role. For carbonate-sourced carbon, the isotopic values were assumed to be 0‰. However, this was accompanied by clear relationships between the isotopic signals and climatic parameters (e.g. discharge and temperature), with heavy $\delta^{13}C_{DIC}$ values occurring under low-flow conditions and light $\delta^{13}C_{DIC}$ values occurring under high-flow conditions, which is in accord with related studies [16, 46, 54]. One hypothesis is that the contribution of lighter $\delta^{13}C_{DIC}$ carbon stored in matrix porosity is higher under warm and wet conditions during the wet period than that found during the dry period [46].

The influx of soil CO_2 produced by soil organic matter degradation can shift ^{13}C-depleted DIC values. As shown in Fig. 7b, there were positive correlations between the content of DIC and DOC during the hydrological year. On the other hand, C_3 plants are widely distributed in this study area, with a mean δ^{13}C value of -27‰. So the δ^{13}C of soil CO_2 in the study area is around -22.6‰, after accounting for the $+4.4$‰ isotopic enrichment

caused by molecular diffusion [54]. Hence, light $\delta^{13}C_{DIC}$ values occur under high-flow conditions, corresponding with higher temperatures than those in the low-flow seasons (Fig. 7c), which may suggest that ^{13}C-depleted DIC can be influenced by soil CO_2, especially under warm and wet conditions. Additionally, DIC contents decreased with increasing discharge (Fig. 7c), which should be ascribed to the shortened fluid transit time during the high-flow seasons, consistent with previous studies in Southwest China [15, 29, 55].

In comparison with atmospheric CO_2, the pCO_2 in the Guijiang River was generally supersaturated, causing large amounts of CO_2 outgassing into the atmosphere. Therefore, the relatively heavier $\delta^{13}C_{DIC}$ values under dry conditions, as compared to those under wet conditions, might be partially attributed to CO_2 outgassing [54]. Because of high CO_2 outgassing with longer residence times during low-flow seasons, the $\delta^{13}C_{DIC}$ values under low-flow conditions are much heavier, whereas there is a shorter residence time during high-flow seasons that may weaken isotopic exchange [54].

The mixing model (i.e. IsoSource) [56] was used to constrain the carbon sources according to the $\delta^{13}C$ values of distinct carbon end-members. The isotopic values were assigned as $-22.6‰$ for biological carbon and 0‰ for carbonate-derived carbon as endmembers, as well as deducting the enrichment of 14.7‰ caused by kinetic fractionation of CO_2 outgassing [57]. The contributions of each source to DIC can be estimated by the following expressions (12–13):

$$\delta^{13}C_{DIC} = \delta^{13}C_{bio} \times a + \delta^{13}C_{carb} \times b - \delta^{13}C_{out} \times c \tag{12}$$

$$a + b + c = 1, \tag{13}$$

where $\delta^{13}C_{bio}$, $\delta^{13}C_{carb}$, and $\delta^{13}C_{out}$ represent the carbon isotopic compositions of biological carbon (DIC_{bio}) and carbonate (DIC_{carb}), and CO_2 outgassing, respectively, a and b indicate the ratios of carbon from biological and carbonate endmembers, and c is the ratio of lost carbon via CO_2 outgassing.

The calculated results showed that the contribution of DIC_{bio} increased from 38% (January of 2014) to 65% (June of 2014), with a mean value of 53% during the hydrological year, displaying a clear positive relationship with increasing discharge (Fig. 7d). These results showed that DIC_{bio} was the dominant factor controlling the behaviors of riverine DIC, and provided strong evidence to support the argument that the exogenous DIC during high-flow seasons was mostly contributed by ^{13}C-depleted soil CO_2. The contribution of DIC_{carb} ranged from 28 to 48%, with a mean of 37%, and showed nearly chemostatic behavior with increases in discharge. The carbon loss from CO_2 outgassing decreased from 26% (January of 2014) to 2%

(June to August of 2014), with a mean of 10%, which may be due to the more limited exchange between water and gas during the wet period relative to that occurring during the dry period [54]. Therefore, DIC in the study river was dominantly controlled by soil CO_2 and its reaction with carbonates. The contributions of various endmembers to DIC can be affected by variations in climatic conditions. These observations were similar to those in other karstic monsoonal rivers [16, 29, 46]. Hence, additional high-frequency sampling (both spatial and temporal) should be conducted to study the isotopic fractionation of DIC under CO_2 outgassing, which have an important impact on the transport of riverine DIC.

Evasion of CO_2 from the river system

To estimate CO_2 evasion flux, the hydrological year was divided into three periods: Period I (October–November of 2013), Period II (January–April of 2014), and Period III (May–September of 2014). Pronounced seasonal variations in CO_2 evasion fluxes were observed throughout the hydrological year. Period II exhibited the strongest CO_2 evasion fluxes (averaging 211 mmol/m^2/days) among the study periods. Meanwhile, a much lower efflux was estimated in Period I (averaging 53 mmol/m^2/days) and the lowest efflux occurred during Period III (averaging 36 mmol/m^2/days) (Table 1). In the Guijiang River, the average value of F_{CO2} (84 mmol/m^2/days) is similar to the Beipan River (78 mmol/m^2/days) [58], but lower than those of the Xijiang River (189.0–356.2 mmol/m^2/days) [19], Amazon River (345.2 mmol/m^2/days) [1], and the Mississippi River (269.9 mmol/m^2/days) [59]. These results further demonstrated that biological

Table 1 Comparison of pCO_2 and CO_2 outgassing of the Guijiang River with rivers worldwide

River	Location	Climate	K (cm/h)	$pCO_{2\ mean}$ (µatm)	F_{CO2} (mmol/m^2/days)	Sources
GJR (I)	China	Subtropical	11	2083	53	This study
GJR (II)	China	Subtropical	16	5162	211	This study
GJR (III)	China	Subtropical	13	1460	36	This study
Beipan	China	Subtropical	8	1287	78	[58]
Xijiang	China	Subtropical	8–15	2600	189.0–356.2	[19]
Yangtze	China	Subtropical	8	1297	38.4–147.9	[60]
Huanghe	China	Subtropical	42.1	2770	856	[61]
Amazon	Brazil	Tropic	15	3320	345.2	[37]
Mississippi	USA	Temperate	16.3	1335	269.9	[59]
Hudson	USA	Temperate	4	1125	16–37	[62]
Ottawa	Canada	Temperate	4	1200	80.8	[8]
Gäddtjärn	Sweden	Boreal	2.1	2266	983	[63]
Lower Mekong	Canada	Boreal	26	611	16	[10]
Auchencorth Moss	UK	Boreal	–	25,418	2.6	[64]
Krycklan	Sweden	Boreal	–	722–24,167	1	[65]

GJR, Guijiang River; I, from October–November of 2013; II, from January–April of 2014; III, from May–September of 2014
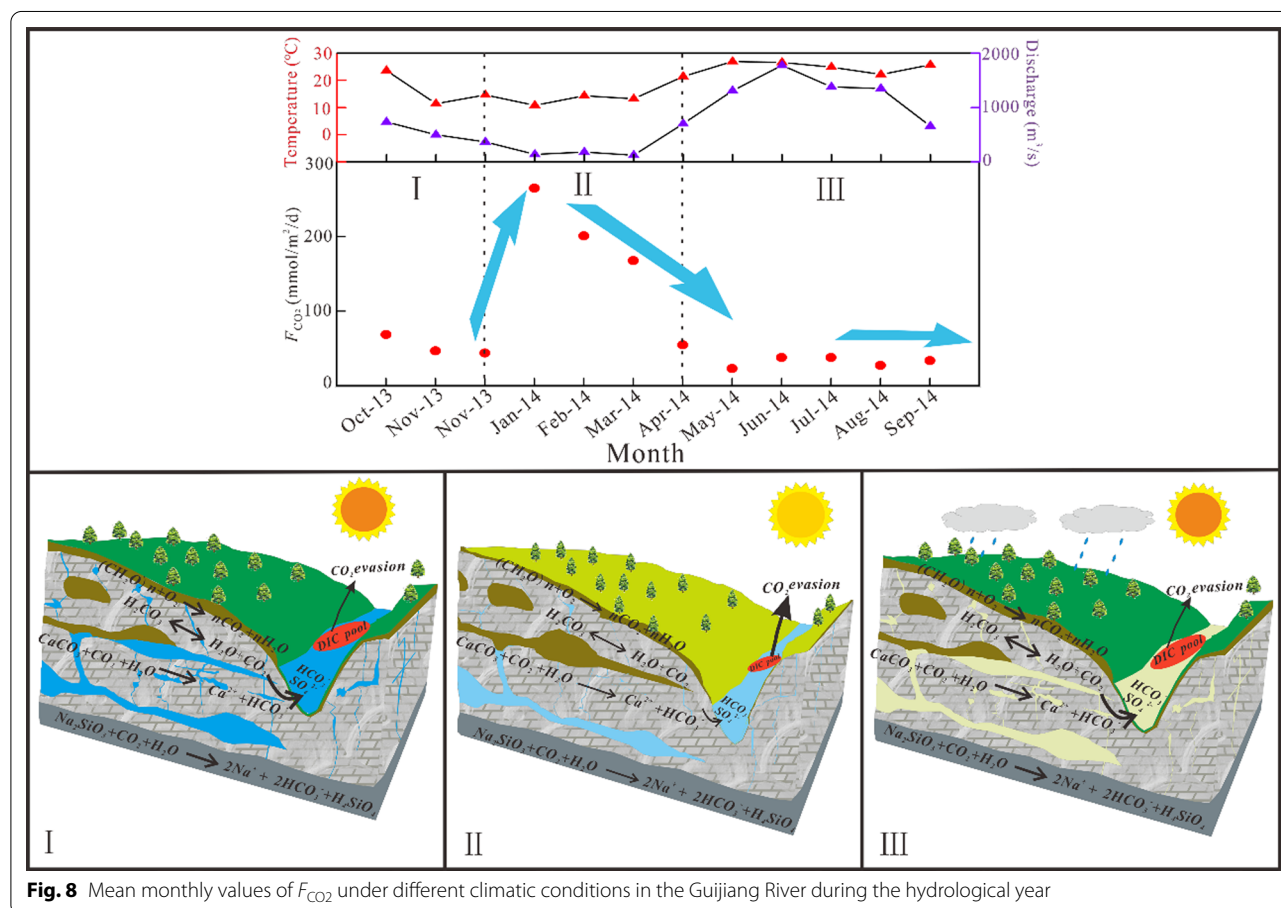
activities increased with the higher temperatures during high-flow seasons, resulting in accelerated chemical weathering rates, and then consuming more soil CO_2. A conceptual model of the seasonal variations in the DIC production, weathering processes, and CO_2 evasion in karst rivers is shown in Fig. 8. Hence, the DIC dynamics under short-term climate variabilities show the significant negative feedback between chemical weathering and global climate change, which needs more attention in future studies.

Conclusions

Based on temporal distributions of riverine dissolved solutes and $\delta^{13}C_{DIC}$ values throughout a hydrological year in the Guijiang River, we found that the dissolved solutes showed obvious temporal variabilities over the hydrological year. Most dissolved solutes with different sources (e.g. geogenic, anthropogenic, and biological solutes) behaved differently with respect to variations in discharge. Our results support the generality of most solutes' $C-Q$ patterns, reflecting chemostatic behaviors and implying consistent source generation and hydro-biogeochemical processes, despite the considerable variations in lithologies and human activity.

Carbonate weathering was the main source of dissolved solutes, and weathering products from carbonates (e.g. Ca^{2+}, Mg^{2+}, and HCO_3^-) showed strong chemostatic behavior when compared to those from silicate weathering (e.g. Na^+ and K^+) in response to changing discharge, which may be due to the rapid dissolution kinetics of carbonate weathering. Meanwhile, both Na^+ and K^+ exhibited dilution effects, implying that silicate-sourced ions are more sensitive to various hydrological conditions than carbonate-sourced ions. Significant positive relationships existed between the weathering rate and variations of climatic conditions, which may be attributed to the presumption that high discharge accelerates solutes transport and high temperature facilitates soil CO_2 production, enhancing rock weathering. Based on the LOADEST program, the CO_2 consumption rates of carbonate and silicate weathering were 14.2×10^9 mol/year and 0.4×10^9 mol/year, respectively. Although the CO_2 consumption rate in the Guijiang River only contributed to a small part of the global CO_2 consumption rate, its CO_2 consumption capacity far exceeded the global mean.

Fig. 8 Mean monthly values of F_{CO2} under different climatic conditions in the Guijiang River during the hydrological year

Liu *et al. Environ Sci Eur*   (2021) 33:53

Page 13 of 15

The IsoSource model was applied to constrain the DIC sources, which demonstrated that soil CO_2 content and its reactions with carbonates were the predominant factors controlling riverine DIC. Meanwhile, compared to the dry period, biological activities increased during the wet period, resulting in high soil CO_2. Temporal variations were also observed in CO_2 fluxes through CO_2 outgassing (F_{CO2}), showing that CO_2 evasion in the wet season was less than that in the dry season, demonstrating further that biological effects become increasingly important with high temperatures. This study provides valuable insights into the carbon dynamics in karst rivers, which can help to improve the understanding of regional and global carbon balance.

Supplementary Information

The online version contains supplementary material available at https://doi.org/10.1186/s12302-021-00495-x.

> **Additional file 1.** Calculation method of the forward model(A), Rates of silicate and carbonate weathering(B), and Flux of CO2 consumption by silicate and carbonate weathering(C).

Authors' contributions
JL and JZ were involved in the investigation, experiments, and manuscript writing. JL, SC, and SX were involved in the data curation and validation. JZ and SL contributed to the study design and review. All authors read and approved the final manuscript.

Availability of data and materials
The datasets used and analyzed during the current study are available from the corresponding author on reasonable request.

Declarations

Ethics approval and consent to participate
Not applicable.

Consent for publication
Not applicable.

Competing interests
The authors declare that they have no competing interests.

Author details
[1] School of Management Science, Guizhou University of Finance and Economics, Guiyang 550025, China. [2] Institute of Surface-Earth System Science, School of Earth System Science, Tianjin University, Tianjin 300072, China. [3] Department of Geography, The University of Hong Kong, Pokfulam Road, Hong Kong, China.

References
1. Li S-L, Xu S, Wang T-J, Yue F-J, Peng T, Zhong J, Wang L-C, Chen J-A, Wang S-J, Chen X, Liu C-Q (2020) Effects of agricultural activities coupled with karst structures on riverine biogeochemical cycles and environmental quality in the karst region. Agr Ecosyst Environ 303:107120. https://doi.org/10.1016/j.agee.2020.107120
2. McClanahan K, Polk J, Groves C, Osterhoudt L, Grubbs S (2016) Dissolved inorganic carbon sourcing using $\delta^{13}C_{DIC}$ from a karst influenced river system. Earth Surf Process Landf 41(3):392–405. https://doi.org/10.1002/esp.3856
3. Li YLJYS, Tank SE, Spence C, Yang D, Bonsal B, McClelland JW, Holmes RM (2018) Seasonal and geographic variation in dissolved carbon biogeochemistry of rivers draining to the Canadian Arctic Ocean and Hudson Bay. J Geophys Res Biogeosci 123(10):3371–3386. https://doi.org/10.1029/2018JG004659
4. Ford D, Williams P (2013) Karst hydrogeology and geomorphology. John Wiley & Sons, Hoboken
5. Xiao J, Jin Z, Zhang F (2013) Geochemical and isotopic characteristics of shallow groundwater within the Lake Qinghai catchment, NE Tibetan Plateau. Quatern Int 313–314:62–73. https://doi.org/10.1016/j.quaint.2013.05.033
6. Gaillardet J, Dupré B, Louvat P, Allègre CJ (1999) Global silicate weathering and CO_2 consumption rates deduced from the chemistry of large rivers. Chem Geol 159(1–4):3–30. https://doi.org/10.1016/S0009-2541(99)00031-5
7. Calmels D, Gaillardet J, Brenot A, France-Lanord C (2007) Sustained sulfide oxidation by physical erosion processes in the Mackenzie River Basin: climatic perspectives. Geology 35(11):1003–1006. https://doi.org/10.1130/G24132A.1
8. Telmer K, Veizer J (1999) Carbon fluxes, pCO2 and substrate weathering in a large northern river basin, Canada: varbon isotope perspectives. Chem Geol 159(1–4):61–86. https://doi.org/10.1016/S0009-2541(99)00034-0
9. Raymond PA, Hartmann J, Lauerwald R, Sobek S, McDonald C, Hoover M, Butman D, Striegl R, Mayorga E, Humborg C, Kortelainen P, Dürr H, Meybeck M, Ciais P, Guth P (2013) Global carbon dioxide emissions from inland waters. Nature 503(7476):355–359. https://doi.org/10.1038/nature12760
10. Li S, Lu XX, Bush RT (2013) CO_2 partial pressure and CO_2 emission in the Lower Mekong River. J Hydrol 504(11):40–56. https://doi.org/10.1016/j.jhydrol.2013.09.024
11. Marescaux A, Thieu V, Borges AV, Garnier J (2018) Seasonal and spatial variability of the partial pressure of carbon dioxide in the human-impacted Seine River in France. Sci Rep 8(1):13961. https://doi.org/10.1038/s41598-018-32332-2
12. Richey JE, Melack JM, Aufdenkampe AK, Ballester VM, Hess LL (2002) Outgassing from Amazonian rivers and wetlands as a large tropical source of atmospheric CO_2. Nature 416(6881):617–620. https://doi.org/10.1038/416617a
13. Zhong J, Li SL, Ibarra D, Ding H, Liu CQ (2020) Solute production and transport processes in Chinese monsoonal rivers:implications for global climate change. Global Biogeochem Cy 34:e2020GB006541. https://doi.org/10.1029/2020GB006541
14. Yang C, Telmer K, Veizer J (1996) Chemical dynamics of the "St. Lawrence" riverine system: δDH2O, δ18OH2O, δ13CDIC, δ34Ssulfate, and dissolved 87Sr/86Sr. Geochim Cosmochim Acta 60(5):851–866. https://doi.org/10.1016/0016-7037(95)00445-9
15. Qin CQ, Li SL, Yue FJ, Xu S, Ding H (2019) Spatiotemporal variations of dissolved inorganic carbon and controlling factors in a small karstic catchment, Southwestern China. Earth Surf Process Landf 44(12):2423–2436. https://doi.org/10.1002/esp.4672
16. Zhong J, Li S-L, Liu J, Ding H, Sun XL, Xu S, Wang TJ, Ellam RM, Liu C-Q (2018) Climate variability controls on CO_2 consumption fluxes and carbon dynamics for monsoonal rivers: evidence from Xijiang River, Southwest China. J Geophys Res Biogeosci 123(8):2553–2567. https://doi.org/10.1029/2018JG004439

Liu *et al. Environ Sci Eur*   (2021) 33:53

Page 14 of 15

17. Clark I, Fritz P (1997) Environmental isotopes in hydrogeology. CRC Press, Boca Raton

18. Liu JK, Han GL (2020) Controlling factors of riverine CO_2 partial pressure and CO_2 outgassing in a large karst river under base flow condition. J Hydrol. https://doi.org/10.1016/j.jhydrol.2020.125638

19. Yao G, Gao Q, Wang Z, Huang X, He T, Zhang Y, Jiao S, Ding J (2007) Dynamics of CO_2 partial pressure and CO_2 outgassing in the lower reaches of the Xijiang River, a subtropical monsoon river in China. Sci Total Environ 376(1–3):255–266. https://doi.org/10.1016/j.scitotenv.2007.01.080

20. Borges AV, Darchambeau F, Teodoru CR, Marwick TR, Tamooh F, Geeraert N, Omengo FO, Guérin F, Lambert T, Morana C, Okuku E, Bouillon S (2015) Globally significant greenhouse-gas emissions from African inland waters. Nature Geosci 8(8):637–642. https://doi.org/10.1038/ngeo2486

21. Moon S, Chamberlain CP, Hilley GE (2014) New estimates of silicate weathering rates and their uncertainties in global rivers. Geochim Cosmochem Acta 134(1):257–274. https://doi.org/10.1016/j.gca.2014.02.033

22. Pu J, Li J, Khadka MB, Martin JB, Zhang T, Yu S, Yuan D (2017) In-stream metabolism and atmospheric carbon sequestration in a groundwater-fed karst stream. Sci Total Environ 579:1343–1355. https://doi.org/10.1016/j.scitotenv.2016.11.132

23. Sun P, He S, Yu S, Pu J, Yuan Y, Zhang C (2021) Dynamics in riverine inorganic and organic carbon based on carbonate weathering coupled with aquatic photosynthesis in a karst catchment, Southwest China. Water Res 189:116658. https://doi.org/10.1016/j.watres.2020.116658

24. Zeng J, Han GL (2020) Preliminary copper isotope study on particulate matter in Zhujiang River, southwest China: application for source identification. Ecotox Environ Safe 198:110663. https://doi.org/10.1016/j.ecoenv.2020.110663

25. Zeng J, Han GL (2020) Tracing zinc sources with Zn isotope of fluvial suspended particulate matter in Zhujiang River, Southwest China. Ecol Indic 118:106723. https://doi.org/10.1016/j.ecolind.2020.106723

26. Xu ZF, Liu C-Q (2007) Chemical weathering in the upper reaches of Xijiang River draining the Yunnan-Guizhou Plateau, Southwest China. Chem Geol 239(1–2):83–95. https://doi.org/10.1016/j.chemgeo.2006.12.008

27. Xu ZF, Liu C-Q (2010) Water geochemistry of the Xijiang basin rivers, South China: chemical weathering and CO_2 consumption. Appl Geochem 25(10):1603–1614. https://doi.org/10.1016/j.apgeochem.2010.08.012

28. Chen P, Lian Y (2016) Modeling of soil loss and its impact factors in the Guijiang Karst River Basin in Southern China. Environ Earth Sci. https://doi.org/10.1007/s12665-016-5288-z

29. Liu J, Zhong J, Ding H, Yue F-J, Li C, Xu S, Li S-L (2020) Hydrological regulation of chemical weathering and dissolved inorganic carbon biogeochemical processes in a monsoonal river. Hydrol Process 34:2780–2792. https://doi.org/10.1002/hyp.13763

30. Pearl River Conservancy Committee (PRCC) (2013) The hydrological yearbooks of Pearl River (in Chinese). PRCC, Beijing (**in Chinese**)

31. Pearl River Conservancy Committee (PRCC) (2014) The hydrological yearbooks of Pearl River (in Chinese). PRCC, Beijing (**in Chinese**)

32. Runkel RL, Crawford CG, Cohn TA (2004) Load Estimator (LOADEST): a FORTRAN Program for Estimating Constituent Loads in Streams and Rivers in U.S. Geological Survey Techniques and Methods 4-A5. United States Geological Survey, Denver, Colorado. https://doi.org/10.3133/tm4A5

33. Booth G, Raymond P, Oh N-H (2007) LoadRunner. New Haven, Conneticut. http://environment.yale.edu/raymond/loadrunner

34. Godsey SE, Kirchner JW, Clow DW (2009) Concentration–discharge relationships reflect chemostatic characteristics of US catchments. Hydrol Process 23(13):1844–1864. https://doi.org/10.1002/hyp.7315

35. Rose LA, Karwan DL, Godsey SE (2018) Concentration–discharge relationships describe solute and sediment mobilization, reaction, and transport at event and longer timescales. Hydrol Process 32(18):2829–2844. https://doi.org/10.1002/hyp.13235

36. Thompson SE, Basu NB, Lascurain J, Aubeneau A, Rao PSC (2011) Relative dominance of hydrologic versus biogeochemical factors on solute export across impact gradients. Water Resour Res 47(10):W00J05.1-W00J05.20. https://doi.org/10.1029/2010WR009605

37. Alin SR, Rasera MFFL, Salimon CI, Richey JE, Holtgrieve GW, Krusche AV, Snidvongs A (2011) Physical controls on carbon dioxide transfer velocity and flux in low-gradient river systems and implications for regional carbon budgets. J Geophys Res Biogeosci 116:G01009. https://doi.org/10.1029/2010JG001398

38. Li SY, Bush RT (2015) Changing fluxes of carbon and other solutes from the Mekong River. Sci Rep 5:16005. https://doi.org/10.1038/srep16005

39. Li S-L, Calmels D, Han G-L, Gaillardet J, Liu C-Q (2008) Sulfuric acid as an agent of carbonate weathering constrained by $\delta^{13}C_{DIC}$: examples from Southwest China. Earth Planet Sci Lett 270(3–4):189–199. https://doi.org/10.1016/j.epsl.2008.02.039

40. Boy J, Valarezo C, Wilcke W (2008) Water flow paths in soil control element exports in an Andean tropical montane forest. Eur J Soil Sci 59(6):1209–1227. https://doi.org/10.1111/j.1365-2389.2008.01063.x

41. Asano Y, Uchida T, Ohte N (2003) Hydrologic and geochemical influences on the dissolved silica concentration in natural water in a steep headwater catchment. Geochim Cosmochim Acta 67(11):1973–1989. https://doi.org/10.1016/S0016-7037(02)01342-X

42. Dobrzyński D (2005) Silica origin and solubility in groundwater from the weathered zone of sedimentary rocks of the Intra-Sudetic Basin. SW Poland Acta Geol Pol 55(4):445–462. https://doi.org/10.1016/j.sedgeo.2003.12.012

43. Wels C, Cornett RJ, Lazerte BD (1991) Hydrograph separation: a comparison of geochemical and isotopic tracers. J Hydrol 122(1–4):253–274. https://doi.org/10.1016/0022-1694(91)90181-G

44. Larssen T, Seip HM, Semb A, Mulder J, Muniz IP, Vogt RD, Lydersen E, Angell V, Tang D, Eilertsen O (1999) Acid deposition and its effects in China: an overview. Environ Sci Policy 2(1):9–24. https://doi.org/10.1016/S1462-9011(98)00043-4

45. NBSC. China Statistical Yearbook (1980−2015). National Bureau of Statistics of China. http://www.stats.gov.cn/. Accessed 15 Jan 2018

46. Li S-L, Liu C-Q, Li J, Lang Y-C, Ding H, Li L (2010) Geochemistry of dissolved inorganic carbon and carbonate weathering in a small typical karstic catchment of Southwest China: isotopic and chemical constraints. Chem Geol 277(3–4):301–309. https://doi.org/10.1016/j.chemgeo.2010.08.013

47. Ollivier P, Hamelin B, Radakovitch O (2010) Seasonal variations of physical and chemical erosion: a three-year survey of the Rhone River (France). Geochim Cosmochim Acta 74(3):907–927. https://doi.org/10.1016/j.gca.2009.10.037

48. Roy S, Gaillardet J, Allègre CJ (1999) Geochemistry of dissolved and suspended loads of the Seine river, France: anthropogenic impact, carbonate and silicate weathering. Geochim Cosmochim Acta 63(9):1277–1292. https://doi.org/10.1016/S0016-7037(99)00099-X

49. Louvat P, Allègre CJ (1997) Present denudation rates on the island of Réunion determined by river geochemistry: basalt weathering and mass budget between chemical and mechanical erosions. Geochim Cosmochem Acta 61(17):3645–3661. https://doi.org/10.1016/S0016-7037(97)00180-4

50. Waldron S, Scott EM, Soulsby C (2007) Stable isotope analysis reveals lower-order river dissolved inorganic carbon pools are highly dynamic. Environ Sci Technol 41(17):6156–6162. https://doi.org/10.1021/es0706089

51. Han GL, Liu C-Q (2004) Water geochemistry controlled by carbonate dissolution: a study of the river waters draining karst-dominated terrain, Guizhou Province. China Chem Geol 204(1–2):1–21. https://doi.org/10.1016/j.chemgeo.2003.09.009

52. Liu B, Liu C-Q, Zhang G, Zhao Z-Q, Li S-L, Hu J, Ding H, Lang Y-C, Li X-D (2013) Chemical weathering under mid- to cool temperate and monsoon-controlled climate: a study on water geochemistry of the Songhuajiang River system, northeast China. Appl Geochem 31:265–278. https://doi.org/10.1016/j.apgeochem.2013.01.015

53. Liu J, Li S-L, Zhong J, Zhu XT, Guo QJ, Lang YC, Han XK (2017) Sulfate sources constrained by sulfur and oxygen isotopic compositions in the upper reaches of the Xijiang River. China Acta Geochim 36(4):611–618. https://doi.org/10.1007/s11631-017-0175-1

54. Amiotte-Suchet P, Aubert D, Probst JL, Gauthier-Lafaye F, Probst A, Andreux F, Viville D (1999) $\delta^{13}C$ pattern of dissolved inorganic carbon in a small granitic catchment: The Strengbach case study (Vosges mountains, France). Chem Geol 159(1–4):129–145. https://doi.org/10.1016/S0009-2541(99)00037-6

55. Wang W-F, Li S-L, Zhong J, Maberly SC, Li C, Wang F-S, Xiao H-Y, Liu C-Q (2019) Climatic and anthropogenic regulation of carbon transport

and transformation in a karst river-reservoir system. Sci Total Environ 707:135628. https://doi.org/10.1016/j.scitotenv.2019.135628

56. Phillips DL, Gregg JW (2003) Source partitioning using stable isotopes: coping with too many sources. Oecologia 136:261–269. https://doi.org/10.1007/s00442-003-1218-3

57. Zhang J, Quay PD, Wilbur DO (1995) Carbon isotope fractionation during gas–water exchange and dissolution of CO_2. Geochim Cosmochim Acta 59(1):107–114. https://doi.org/10.1016/0016-7037(95)91550-D

58. Zou J (2016) Sources and dynamics of inorganic carbon within the upper reaches of the Xi River Basin, Southwest China. PLoS ONE 11(8):e0160964. https://doi.org/10.1371/journal.pone.0160964

59. Dubois KD, Lee D, Veizer J (2010) Isotopic constraints on alkalinity, dissolved organic carbon, and atmospheric carbon dioxide fluxes in the Mississippi River. J Geophys Res Biogeosci 115:G02018. https://doi.org/10.1029/2009JG001102

60. Wang FS, Wang Y, Zhang J, Xu H, Wei X (2007) Human impact on the historical change of CO_2 degassing flux in River Changjiang. Geochem Trans. https://doi.org/10.1186/1467-4866-8-7

61. Ran L, Lu XX, Yang H, Li L, Yu R, Sun H, Han J (2015) CO_2 outgassing from the Yellow River network and its implications for riverine carbon cycle. J Geophys Res Biogeosci 120(7):1334–1347. https://doi.org/10.1002/2015JG002982

62. Raymond PA, Caraco NF, Cole JJ (1997) Carbon dioxide concentration and atmospheric flux in the Hudson River. Estuaries 20(2):381–390. https://doi.org/10.2307/1352351

63. Kokic J, Wallin MB, Chmiel HE, Denfeld BA, Sobek S (2015) Carbon dioxide evasion from headwater systems strongly contributes to the total export of carbon from a small boreal lake catchment. J Geophys Res Biogeosci 120(1):13–28. https://doi.org/10.1002/2014JG002706

64. Dinsmore KJ, Billett MF, Skiba UM, Rees RM, Drewer J, Helfter C (2010) Role of the aquatic pathway in the carbon and greenhouse gas budgets of a peatland catchment. Glob Change Biol 16(10):2750–2762. https://doi.org/10.1111/j.1365-2486.2009.02119.x

65. Wallin MB, Grabs T, Buffam I, Laudon H, Agren A, Oquist MG, Bishop K (2013) Evasion of CO_2 from streams–the dominant component of the carbon export through the aquatic conduit in a boreal landscape. Glob Change Biol 19(3):785–797. https://doi.org/10.1111/gcb.12083

Publisher's Note